Nb and Ta incorporation and fractionation in titanian pargasite and kaersutite: Crystal-chemical constraints and implications for natural systems

Article *in* Earth and Planetary Science Letters · March 2000

DOI: 10.1016/S0012-821X(00)00004-2

CITATIONS
239

READS
327

6 authors, including:

Massimo Tiepolo
University of Milan
190 PUBLICATIONS **6,228** CITATIONS
SEE PROFILE

Riccardo Vannucci
University of Pavia
223 PUBLICATIONS **8,117** CITATIONS
SEE PROFILE

Stephen F. Foley
Macquarie University
210 PUBLICATIONS **13,246** CITATIONS
SEE PROFILE

Alberto Zanetti
Italian National Research Council
200 PUBLICATIONS **4,460** CITATIONS
SEE PROFILE

ELSEVIER

Earth and Planetary Science Letters 176 (2000) 185–201

EPSL

www.elsevier.com/locate/epsl

Nb and Ta incorporation and fractionation in titanian pargasite and kaersutite: crystal–chemical constraints and implications for natural systems

M. Tiepolo [a,*], R. Vannucci [a,b], R. Oberti [b], S. Foley [c], P. Bottazzi [b], A. Zanetti [b]

[a] *Dipartimento di Scienze della Terra, Università di Pavia, Via Ferrata 1, I-27100 Pavia, Italy*
[b] *CNR-Centro di Studio per la Cristallochimica e la Cristallografia (CSCC), Via Ferrata 1, I-27100 Pavia, Italy*
[c] *Mineralogisch-Petrologisches Institut, Universität Göttingen, Goldschmidtstrasse 1, D-37077 Göttingen, Germany*

Received 16 August 1999; received in revised form 14 December 1999; accepted 29 December 1999

Abstract

New partition coefficients between liquid and pargasitic/kaersutitic amphiboles ($^{Amph/L}D_{Nb,Ta}$) experimentally determined for Nb and Ta at upper-mantle conditions, combined with single-crystal structure refinement of the synthesised amphiboles, show that $^{Amph/L}D_{Nb,Ta}$ are strongly dependent on the structure and composition of both amphibole and melt. The correlation of the $^{Amph/L}D_{Nb,Ta}$ with the amphibole oxy-component is explained by the ordering of Nb and Ta at the M1 site, contributing with the fraction of Ti at M1 to locally balance the $^{O3}O^{2-} \leftrightarrow {}^{O3}(OH)^{-}$ substitution. In our set of dehydrogenated amphiboles, variations in the SiO_2 content of the melt from 41.5 to 54.6 correspond to a six-fold increase of the $^{Amph/L}D_{Nb,Ta}$, in which $^{Amph/L}D_{Nb}$ varies from 0.14 to 0.71 and $^{Amph/L}D_{Ta}$ from 0.11 to 0.54. Partition coefficients for Nb and Ta abruptly increase in Ti-depleted compositions ($^{Amph/L}D_{Nb}$ up to 1.63 and $^{Amph/L}D_{Ta}$ to 1.00). The ratio of D_{Nb} to D_{Ta} ($^{Amph/L}D_{Nb/Ta}$) varies from 0.71 to 1.63, and is a function of the M1 site dimension, which in turn depends on its Fe, Mg and Ti contents. The observed variations can be explained by assuming that the ionic radius of Nb is ($\sim$0.01–0.02 Å) larger than that of Ta, contrary to the common assumption that they are both equal to 0.64 Å. We calibrated a simplified model for the prediction of $^{Amph/L}D_{Nb/Ta}$ values shown to be negatively related mainly to *mg*# [Mg/(Mg+Fe)] and to Ti content. High-*mg*# amphiboles have $^{Amph/L}D_{Nb/Ta}$ close to unity, so the low Nb/Ta found in convergent margin volcanics and in the continental crust cannot be explained by the involvement of amphibole in the mantle wedge. Amphibole in the subducting slab may have lower *mg*# and consequently high Nb/Ta values, and thus may give rise to subchondritic Nb/Ta values in coexisting melts. Nb/La is also negatively correlated with *mg*#, and strongly increases in Ti-depleted compositions.

Keywords: trace elements; partitioning; amphibole group; niobium; tantalum; experimental studies; island arcs; volcanic rocks

1. Introduction

Advances in analytical techniques have led to increased geochemical importance of Nb and Ta

* Corresponding author. Tel.: +39-382-505867; Fax: +39-382-505890; E-mail: tiepolo@crystal.unipv.it

0012-821X/00/$ – see front matter
PII: S0012-821X(00)00004-2

during the last few years, both in terms of the internal Nb/Ta ratio and of the fractionation of these elements from other nominally strongly incompatible trace elements. It has long been recognised that the degree of incompatibility of Nb and Ta is close to that of Th, U, La and Ce in most oceanic basalts [1,2], whereas they have anomalously low concentrations and consequently show negative anomalies in trace-element patterns (and low Nb/U and Nb/La) for igneous rocks of convergent margins and for the bulk continental crust [3,4]. Furthermore, the Nb/Ta ratio has near-chondritic values (around 18) only in MORB and OIB (although significantly lower values were also documented [5]), considerably lower values in convergent margins and in the continental crust (12–14; [4,6,7], Eggins, personal communication) and even higher values in some island-arc volcanics [8]. Although these characteristics have been commonly used as diagnostic for a subduction environment and thus applied as tectonic indicators for rocks in earlier parts of the Earth's history, there is increasing recognition that they occur 'out-of-place' as components in the genesis of intra-plate continental [9,10] and some oceanic [11,12] basalts.

However, the underlying mechanism controlling the behaviour of Nb and Ta is poorly understood. Although the fractionation of Nb and Ta from Th, U, La and Ce appears to indicate the involvement of a phase which selectively incorporates Nb and Ta, current data exclude all the common mantle minerals (Cpx, Opx, Ol, Gt, Sp) as the Nb and Ta hosts. The presence of Ti-bearing phases (e.g., rutile or sphene) is commonly invoked in the intra-plate and sub-arc mantle or in the subducting slab to explain Nb and Ta fractionation and depletion. Partition coefficients for Nb and Ta are very high (100–3500) for rutile/fluid and rutile/melt pairs [13–16], but the low modal abundance of these phases may nevertheless preclude their controlling the Nb–Ta signature [17]. Mantle peridotites commonly do not contain rutile due to a reaction with olivine to form ilmenite and orthopyroxene [18], and Ti is highly soluble in mafic melts, so that Ti minerals are unlikely to remain stable after the onset of melting [19].

Table 1
Experimental conditions and compositions for the samples of this work

Sample	Code	T_{sl} (°C)	T_{eq} (°C)
1	A-N-melt*	1245	1015
2	A-N-melt	1245	1015
3	A-N-synth	1245	1015
4	A-K-1.00	1245	1015
5	A-K-0.81	1245	1015
6	A-K-0.71	1245	1015
7	A-M-0.45	1245	950
8	B-N-melt	1245	1015
9	B-T-0.89	1245	975
10	B-T-0.89	1245	1015
11	B-T-0.89	1245	1035
12	B-T-0.89	1245	1055
13	B-T-0.94	1245	1015
14	B-T-0.94	1245	1035
15	B-T-0.94	1245	1055
16	B-T-0.94	1245	1075
17	B-T-0.97	1245	975
18	B-T-0.97	1245	1015
19	B-M-0.45	1245	1045
20	B-M-0.75	1245	1050
21	B-M-0.90	1245	1050
22	B-M-1.00	1255	1070
23	B-K-1.00	1245	1030
24	B-K-0.50	1245	1030
25	B-K-0.81	1245	1030

The code is a combination of (1) the composition of the starting material (A = olivine alkali-basalt 472213a, B = basanite WR13-141); (2) the vector along which the composition was varied (N = natural composition, $K = K_2O/(K_2O+Na_2O)$, $M = MgO/(MgO+FeO^*)$, $T = SiO_2/(SiO_2+TiO_2)$; (3) the value of the A/(A+B) ratio between the two oxides that were varied. T_{sl} is the initial temperature from which the experiments were cooled slowly to the equilibrium run temperature (T_{eq}); duration = 13 h.

Ionov and Hofmann [20] described amphibole from mantle xenoliths that are both highly enriched in Nb and Ta relative to Th, U, La and Ce, and highly variable in Nb/Ta (11–90). These authors suggested that amphibole may be an important phase controlling Nb and Ta in the sub-arc mantle. However, all experimentally determined values reported so far for the partition coefficients of Nb and Ta in amphibole [21–23] are too low to favour the interpretation that amphibole can act as a retentive phase during partial melting or subsequent element-filtering processes.

We present and discuss an extensive new exper-

Table 2
Unit-cell parameters and selected refinement results for the synthesised amphibole of this work

Sample	SEQ*	R_{obs}	R_{all}	*a*	*b*	*c*	β	V	⟨M1−O⟩	⟨M2−O⟩	⟨M3−O⟩	⟨M4−O⟩
1	834	1.4	2.5	9.861 (3)	18.023 (7)	5.307 (3)	105.21 (4)	910.1	2.079	2.054	2.072	2.487
2	888	1.9	4.5	9.846 (5)	18.042 (10)	5.316 (2)	105.10 (3)	911.7	2.081	2.048	2.087	2.486
3	835	1.4	3.5	9.858 (2)	18.031 (4)	5.307 (2)	105.13 (2)	910.5	2.080	2.053	2.075	2.487
4	935	2.0	7.9	9.806 (8)	18.026 (15)	5.308 (2)	104.91 (4)	906.7	2.077	2.053	2.079	2.483
5	934	1.9	5.5	9.838 (8)	18.025 (21)	5.308 (5)	105.01 (6)	909.2	2.082	2.052	2.074	2.486
6	933	1.9	5.9	9.850 (4)	18.046 (11)	5.316 (2)	105.10 (3)	912.2	2.083	2.050	2.082	2.487
7	837	1.6	2.7	9.880 (4)	18.095 (6)	5.322 (2)	105.13 (3)	918.5	2.090	2.050	2.094	2.492
8	842	2.1	4.7	9.836 (4)	18.043 (10)	5.320 (2)	105.02 (2)	911.9	2.081	2.043	2.090	2.489
9	884	1.7	3.0	9.853 (7)	18.060 (13)	5.314 (7)	105.07 (7)	913.0	2.083	2.051	2.088	2.490
10	863	2.0	3.8	9.872 (4)	18.070 (7)	5.321 (4)	105.16 (4)	916.1	2.081	2.052	2.086	2.494
11	862	1.5	2.8	9.880 (6)	18.073 (11)	5.318 (3)	105.19 (4)	916.4	2.082	2.058	2.085	2.496
12	861	1.6	2.7	9.873 (4)	18.060 (7)	5.315 (2)	105.17 (3)	914.8	2.079	2.056	2.083	2.496
13	893	1.8	4.4	9.865 (5)	18.072 (7)	5.313 (3)	105.04 (4)	914.8	2.083	2.062	2.082	2.497
15	894	1.5	2.9	9.856 (3)	18.057 (6)	5.316 (3)	105.07 (3)	913.6	2.080	2.054	2.085	2.492
16	902	1.4	3.0	9.893 (2)	18.036 (4)	5.303 (2)	105.20 (2)	913.1	2.075	2.066	2.064	2.499
17	889	1.7	4.3	9.862 (4)	18.063 (6)	5.319 (3)	105.06 (3)	915.0	2.088	2.046	2.092	2.492
18	877	2.0	4.4	9.857 (6)	18.037 (12)	5.310 (4)	105.09 (4)	911.5	2.086	2.047	2.087	2.488
19	878	1.6	3.4	9.862 (3)	18.067 (6)	5.316 (3)	105.11 (3)	914.5	2.082	2.056	2.086	2.494
20	879	2.2	5.4	9.871 (4)	18.028 (8)	5.307 (2)	105.24 (2)	911.1	2.075	2.055	2.074	2.494
21	890	1.5	3.1	9.888 (3)	18.023 (5)	5.308 (2)	105.31 (2)	912.4	2.072	2.056	2.068	2.496
22	864	1.4	2.9	9.903 (4)	17.995 (8)	5.304 (3)	105.44 (3)	911.3	2.071	2.055	2.062	2.496
23	887	1.9	5.7	9.839 (3)	18.060 (5)	5.314 (2)	105.03 (2)	912.0	2.078	2.059	2.082	2.491
24	885	1.7	3.5	9.869 (3)	18.049 (7)	5.310 (3)	105.16 (3)	912.9	2.080	2.059	2.078	2.494
25	903	1.3	1.8	9.919 (2)	18.080 (4)	5.313 (1)	105.26 (2)	919.2	2.084	2.069	2.080	2.502

R = disagreement indices (%) at convergence for all the reflections (R_{all}) and for those used in the least-square procedure (R_{obs}; $I > 5\sigma_I$)
*Sequence number in the CSCC database.

imental data set on the partitioning of Nb and Ta between pargasitic and kaersutitic amphiboles and melts from basanitic and alkali-basaltic systems under upper-mantle conditions [24]. We also present data for La, which enable assessment of Nb depletion relative to elements of similar incompatibility. By combining current knowledge on amphibole crystal-chemistry and the results of single-crystal structure refinement, we suggest that amphibole may determine the Nb and Ta signature of magmas during mineral/melt fractionation processes in the upper mantle.

2. Experimental and analytical procedures

2.1. Synthesis

An alkali-olivine basalt from Hessen, Germany, [[25]; sample 472213a] and a basanite from Mt. Melbourne Volcanic Field, Victoria Land, Antartica ([26]; sample WR13–141) were selected as starting materials. These compositions were reproduced by mixing oxides and carbonates of Si, Mg, Fe, Al, Ti, Ca, Na, and K. All carbonates were reduced to oxides by sintering before the experiment, and a mixture of Fe^0 and Fe_2O_3 was used in order to obtain appropriate Fe^{2+} and Fe^{3+} proportions. The ratios K/(Na+Ca), Mg/(Mg+Fe) and Ti/(Ti+Si) were varied systematically in the starting mixtures by adding the appropriate proportions of the relevant oxides so as to maximise the compositional and structural range of amphiboles to encompass a broad range of partitioning behaviour. The starting materials were doped with a mixture of trace elements added in solid form at abundances designed to achieve optimal analytical conditions with counting statistics on both amphibole and glass of better than 2% during secondary ion mass spectrom-

Table 3
Amphibole compositions, unit formulas calculated on the basis of 24 (O, OH, F, Cl) and site partitioning for Ti (apfu)

	1	2	3	4	5	6	7	8	9	10	11	12	13	14	15
SiO_2	40.72	38.06	40.63	39.36	39.86	39.64	38.71	40.26	38.73	38.06	38.87	39.89	40.08	39.55	39.24
TiO_2	4.06	4.98	3.98	5.33	5.44	5.19	3.66	5.99	4.94	5.78	5.71	5.72	5.03	4.39	5.59
Al_2O_3	15.02	15.53	14.69	14.80	15.53	15.44	15.40	13.63	14.94	15.00	15.94	14.53	13.87	13.66	15.22
Cr_2O_3	0.01	0.01	0.02	0.01	–	0.01	–	0.04	0.01	–	–	–	0.01	0.03	0.01
FeOT	8.62	15.29	9.02	12.88	11.78	13.80	19.72	14.46	16.35	14.26	13.84	12.94	15.33	15.27	13.75
MnO	0.12	–	0.13	0.01	–	0.01	0.01	0.22	0.01	–	–	0.01	–	–	0.01
MgO	14.48	9.13	14.11	11.67	11.18	10.36	6.35	9.96	8.93	9.04	9.92	11.02	10.50	9.30	10.62
CaO	10.51	9.71	10.08	8.84	9.20	9.91	9.95	9.42	9.66	9.86	10.37	10.28	9.56	10.09	9.62
Na_2O	2.59	2.46	2.85	3.73	3.39	2.80	2.55	3.16	2.93	3.04	3.00	2.75	2.85	3.15	2.68
K_2O	1.33	1.55	1.14	0.03	0.747	1.20	1.66	1.30	1.19	1.37	1.38	1.44	1.18	1.27	1.42
H_2O	1.00	0.95	1.26	1.01	1.04	0.89	1.02	1.00	0.99	0.95	0.97	0.99	0.85	0.91	0.90
F	0.02	0.01	0.01	0.03	0.04	0.03	0.21	–	0.04	0.07	0.07	0.04	0.08	0.03	0.04
-O = F	–	–	–	−0.01	−0.02	−0.01	−0.09	–	−0.02	−0.02	−0.02	−0.02	−0.02	−0.04	−0.01
Total	98.48	97.68	97.92	97.68	98.19	99.27	99.15	99.44	98.70	97.41	100.05	99.59	99.32	97.61	99.08
Si	6.01	5.88	6.05	5.96	6.01	5.97	6.00	6.08	5.93	5.87	5.81	5.98	6.05	6.08	5.92
Al	1.99	2.12	1.95	2.04	1.99	2.03	2.00	1.92	2.07	2.13	2.19	2.02	1.95	1.92	2.08
Σ T	8.00	8.00	8.00	8.00	8.00	8.00	8.00	8.00	8.00	8.00	8.00	8.00	8.00	8.00	8.00
Al	0.63	0.70	0.64	0.60	0.77	0.71	0.81	0.51	0.62	0.60	0.62	0.55	0.52	0.55	0.63
Fe^{3+}+Cr	0.46	0.33	0.20	0.27	0.05	0.28	0.27	0.21	0.38	0.36	0.42	0.24	0.46	0.59	0.31
Ti	0.45	0.58	0.45	0.61	0.62	0.59	0.43	0.68	0.57	0.67	0.64	0.65	0.57	0.51	0.64
Mg	3.01	2.02	2.96	2.47	2.40	2.16	1.47	2.25	1.95	2.08	2.21	2.38	2.26	2.13	2.26
Fe^{2+}	0.45	1.37	0.75	1.05	1.16	1.26	2.02	1.35	1.48	1.29	1.11	1.18	1.19	1.22	1.16
Σ M(1.2.3)	5.00	5.00	5.00	5.00	5.00	5.00	5.00	5.00	5.00	5.00	5.00	5.00	5.00	5.00	5.00
Mg	0.18	0.08	0.17	0.16	0.11	0.15	–	–	0.08	–	–	0.07	0.10	–	0.12
Fe^{2+}+Mn	0.17	0.28	0.19	0.31	0.27	0.20	0.26	0.30	0.24	0.19	0.20	0.21	0.29	0.15	0.26
Ca	1.65	1.60	1.60	1.43	1.49	1.60	1.65	1.52	1.58	1.63	1.67	1.65	1.55	1.67	1.56
Na	–	0.04	0.04	0.10	0.13	0.05	0.09	0.18	0.10	0.18	0.13	0.07	0.06	0.18	0.06
Σ M4	2.00	2.00	2.00	2.00	2.00	2.00	2.00	2.00	2.00	2.00	2.00	2.00	2.00	2.00	2.00
Na	0.75	0.70	0.75	0.99	0.86	0.77	0.67	0.75	0.77	0.73	0.74	0.72	0.77	0.76	0.73
K	0.25	0.30	0.25	0.01	0.14	0.23	0.33	0.25	0.23	0.27	0.26	0.28	0.23	0.25	0.27
Σ A	1.00	1.00	1.00	1.00	1.00	1.00	1.00	1.00	1.00	1.00	1.00	1.00	1.00	1.01	1.00
OH	0.98	0.97	1.25	1.04	1.04	0.90	1.05	1.01	1.01	0.98	0.97	0.99	0.86	0.93	0.90
F	0.01	0.01	0.01	0.02	0.03	0.02	0.11	–	0.03	0.03	0.03	0.03	0.03	0.03	0.03
O	1.01	1.02	0.74	0.94	0.93	1.08	0.84	0.99	0.96	0.99	1.00	0.98	1.11	1.04	1.07
Σ X	2.00	2.00	2.00	2.00	2.00	2.00	2.00	2.00	2.00	2.00	2.00	2.00	2.00	2.00	2.00
$\Delta ss_{M(1,2,3)}$	−0.06	1.20	1.69	1.00	1.25	2.12	4.91	0.02	1.86	1.77	1.02	0.52	0.64	–	1.09
$\Delta ss_{M(4)}$	−0.03	0.54	0.85	0.47	0.59	0.95	0.70	−0.13	0.80	0.30	0.17	0.24	0.29	–	0.50
Δss_{A}	0.37	0.29	0.71	−0.08	−0.09	0.34	0.25	0.60	0.49	0.64	0.60	0.48	0.62	–	0.28
mg#	0.75	0.52	0.74	0.62	0.63	0.57	0.36	0.55	0.49	0.53	0.56	0.60	0.55	0.52	0.58
na#	0.75	0.71	0.76	0.99	0.88	0.78	0.70	0.79	0.79	0.77	0.77	0.74	0.78	0.79	0.75
^{M1}Ti	0.33	0.43	0.36	0.47	0.44	0.46	0.31	0.50	0.48	0.52	0.49	0.49	0.49	0.44	0.53
^{M2}Ti	0.12	0.15	0.08	0.13	0.17	0.12	0.12	0.18	0.09	0.15	0.15	0.15	0.08	0.07	0.10
^{M3}Ti	–	–	–	–	–	–	–	–	–	–	–	–	–	–	–

The differences between the group-site scatterings obtained from the structure refinement and those calculated from the unit formulas (Δss, electrons pfu) testify the quality of the crystal–chemical characterisation. Sample sequence as in Table 1. The clinopyroxene from sample 2 is also included.

	16	17	18	19	20	21	22	23	24	25		Cpx 2
SiO_2	43.44	38.70	38.60	37.97	39.75	40.44	40.40	39.82	39.45	40.40	SiO_2	51.98
TiO_2	3.86	2.94	3.84	5.41	6.35	6.11	6.17	6.04	5.10	4.20	TiO_2	1.03
Al_2O_3	12.35	15.16	15.56	14.53	14.29	14.36	15.27	14.27	14.74	13.41	Al_2O_3	6.60
Cr_2O_3	0.01	–	0.01	–	–	0.02	–	–	0.01	0.03	Cr_2O_3	0.04
FeOT	4.82	19.06	16.56	15.96	7.93	3.77	–	14.27	13.70	12.25	FeOT	6.02
MnO	0.01	0.02	0.01	–	–	–	–	0.02	–	0.01	MnO	–
MgO	18.17	8.14	9.34	9.14	13.89	16.39	18.39	10.47	10.91	12.64	MgO	15.23
CaO	11.32	9.57	9.71	9.92	10.71	11.01	11.51	10.05	10.40	11.19	CaO	20.21
Na_2O	2.62	2.96	2.79	2.74	2.87	3.16	3.21	4.04	3.22	2.36	Na_2O	0.94
K_2O	1.55	1.27	1.36	1.53	1.47	1.14	1.16	0.05	0.94	1.77		
H_2O	1.06	1.23	1.25	0.88	1.08	1.16	1.42	1.00	0.99	1.23		
F	1.66	0.06	0.03	0.06	0.02	0.02	0.03	0.03	0.03	0.02		
-O = F	−0.06	−0.03	−0.01	−0.03	−0.01	−0.01	−0.01	−0.01	−0.01	−0.01		
Total	100.81	99.08	99.05	98.12	98.35	97.57	97.55	100.05	99.48	99.50	Total	102.05
Si	6.23	5.93	5.87	5.84	5.91	5.94	5.86	5.93	5.90	6.03	Si	1.86
Al	1.77	2.07	2.13	2.16	2.09	2.06	2.14	2.07	2.10	1.97	Al	0.14
Σ T	8.00	8.00	8.00	8.00	8.00	8.00	8.00	8.00	8.00	8.00	Σ T	2.00
Al	0.31	0.66	0.67	0.47	0.42	0.43	0.47	0.44	0.50	0.38	Al	0.14
Fe^{3+}+Cr	–	0.56	0.38	0.61	0.27	0.25	–	0.44	0.57	0.43	Fe^{3+}+Cr	0.01
Ti	0.42	0.34	0.44	0.63	0.71	0.67	0.67	0.68	0.57	0.47	Ti	0.03
Mg	3.75	1.86	2.11	2.09	2.98	3.49	3.86	2.30	2.41	2.73	Mg	0.81
Fe^{2+}	0.51	1.58	1.41	1.20	0.62	0.16	–	1.14	0.96	0.99	Fe^{2+}	0.01
Σ M(1.2.3)	5.00	5.00	5.00	5.00	5.00	5.00	5.00	5.00	5.00	5.00	Σ M1	1.00
Mg	0.12	–	–	–	0.10	0.10	0.12	0.02	0.03	0.08	Mg	–
Fe^{2+}+Mn	0.07	0.30	0.33	0.25	0.09	0.06	–	0.19	0.19	0.11	Fe^{2+}+Mn	0.16
Ca	1.74	1.57	1.58	1.63	1.70	1.73	1.79	1.61	1.67	1.79	Ca	0.77
Na	0.07	0.13	0.09	0.12	0.11	0.11	0.09	0.18	0.11	0.02	Na	0.07
Σ M4	2.00	2.00	2.00	2.00	2.00	2.00	2.00	2.00	2.00	2.00	Σ M2	1.00
Na	0.65	0.75	0.74	0.70	0.72	0.79	0.79	0.99	0.82	0.66		
K	0.28	0.25	0.26	0.30	0.28	0.21	0.21	0.01	0.18	0.34		
Σ A	0.93	1.00	1.00	1.00	1.00	1.00	1.00	1.00	1.00	1.00		
OH	1.01	1.26	1.27	0.91	1.07	1.14	1.38	0.99	0.99	1.22		
F	0.75	0.04	0.03	0.04	0.01	0.01	0.02	0.01	0.01	0.01		
O	0.24	0.70	0.70	1.05	0.92	0.85	0.61	1.00	1.00	0.77		
Σ X	2.00	2.00	2.00	2.00	2.00	2.00	2.01	2.00	2.00	2.00		
$\Delta ss_{M(1,2,3)}$	0.84	1.59	1.99	1.15	−0.80	0.50	0.19	0.33	−0.04	0.41		
$\Delta ss_{M(4)}$	0.46	0.71	0.09	0.21	−0.39	0.26	0.43	0.14	−0.02	0.19		
Δss_A	0.82	0.15	1.16	0.58	0.65	0.67	0.40	0.22	0.69	0.12		
mg#	0.87	0.43	0.50	0.50	0.76	0.89	1.00	0.57	0.59	0.65		
na#	0.72	0.78	0.76	0.73	0.75	0.81	0.81	0.99	0.84	0.67		
^{M1}Ti	0.12	0.24	0.31	0.53	0.45	0.42	0.32	0.45	0.41	0.38		
^{M2}Ti	0.30	0.10	0.13	0.10	0.15	0.11	0.25	0.23	0.16	0.09		
^{M3}Ti	–	–	–	–	0.11	0.14	0.10	–	–	–		

Table 4
Average compositions of glasses in the experimental charges obtained by EMP analyses and SIMS (H_2O)

Sample	SiO_2	TiO_2	Al_2O_3	FeO	MgO	CaO	Na_2O	K_2O	H_2O	Tot
1	46.26 ± 1.52	2.48 ± 0.05	15.96 ± 0.52	9.37 ± 0.31	4.39 ± 0.58	6.37 ± 0.24	1.37 ± 0.27	1.93 ± 0.11	6.15	97.86
2	52.25 ± 0.72	1.71 ± 0.24	18.91 ± 0.07	9.80 ± 0.40	1.98 ± 0.17	4.60 ± 0.21	3.81 ± 0.05	3.48 ± 0.12	3.31 ± 0.14	101.84
3	44.93 ± 1.43	2.77 ± 0.13	15.19 ± 0.29	10.11 ± 0.13	5.15 ± 0.53	6.61 ± 0.19	1.79 ± 0.44	1.59 ± 0.18	4.69 ± 1.17	96.15
4	50.40 ± 0.48	2.07 ± 0.04	18.62 ± 0.24	9.92 ± 0.04	2.25 ± 0.13	4.88 ± 0.12	4.05 ± 0.65	0.06 ± 0.02	–	93.96
5	52.37 ± 0.20	1.63 ± 0.34	18.68 ± 0.04	8.86 ± 0.01	2.16 ± 0.04	4.79 ± 0.02	3.01 ± 0.19	1.70 ± 0.02	–	94.06
6	53.02 ± 0.51	1.54 ± 0.03	18.61 ± 0.10	9.20 ± 0.05	1.75 ± 0.21	4.37 ± 0.08	3.18 ± 0.22	2.70 ± 0.06	–	95.63
7	51.88 ± 2.00	1.27 ± 0.13	17.09 ± 0.22	11.36 ± 0.18	1.02 ± 0.07	4.33 ± 0.16	2.78 ± 0.07	3.53 ± 0.07	–	96.15
8	52.22 ± 0.41	1.17 ± 0.10	19.38 ± 0.25	8.43 ± 0.08	1.83 ± 0.11	2.54 ± 0.16	5.39 ± 0.08	4.12 ± 0.09	–	96.26
9	54.60 ± 1.37	1.42 ± 0.14	17.96 ± 0.93	7.69 ± 0.50	1.50 ± 0.35	2.93 ± 0.14	3.89 ± 0.16	3.51 ± 0.16	–	97.24
10	48.15 ± 0.83	2.54 ± 0.56	15.65 ± 0.84	9.40 ± 0.60	2.20 ± 0.90	3.47 ± 0.58	7.56 ± 0.60	3.37 ± 0.20	3.27 ± 0.76	100.71
11	47.00 ± 0.94	2.96 ± 0.26	15.12 ± 0.44	10.83 ± 0.36	3.12 ± 0.94	4.30 ± 0.52	6.85 ± 0.57	3.08 ± 0.17	3.58 ± 0.29	101.04
12	45.74 ± 2.04	4.17 ± 1.83	14.74 ± 0.90	12.19 ± 0.99	3.39 ± 1.53	4.37 ± 0.80	6.73 ± 0.95	2.82 ± 0.35	–	103.54
13	48.55 ± 1.40	2.55 ± 0.08	18.09 ± 0.05	12.09 ± 0.29	2.65 ± 0.16	4.53 ± 0.14	4.12 ± 0.21	2.77 ± 0.36	2.76 ± 0.01	100.79
14	54.64 ± 0.39	1.43 ± 0.05	17.50 ± 0.26	7.03 ± 0.13	1.31 ± 0.03	2.87 ± 0.05	4.46 ± 0.27	3.56 ± 0.05	4.46 ± 0.12	98.49
15	50.40 ± 2.13	2.11 ± 0.04	15.50 ± 0.54	11.11 ± 0.42	2.48 ± 0.19	3.90 ± 0.17	3.49 ± 0.26	2.84 ± 0.17	3.03 ± 0.06	98.75
16	41.53 ± 0.30	5.39 ± 0.08	13.22 ± 0.10	8.01 ± 0.18	7.98 ± 0.09	9.54 ± 0.13	2.99 ± 0.33	1.38 ± 0.06	3.65 ± 0.04	94.95
17	53.20 ± 1.85	0.44 ± 0.04	19.42 ± 0.19	9.25 ± 0.28	1.36 ± 0.06	2.76 ± 0.07	5.15 ± 0.33	3.42 ± 0.23	3.03 ± 0.08	101.06
18	50.47 ± 1.79	0.75 ± 0.08	18.52 ± 0.28	11.62 ± 0.27	1.93 ± 0.09	3.67 ± 0.13	4.17 ± 0.20	3.27 ± 0.11	3.53 ± 0.09	100.88
19	48.10 ± 0.61	2.35 ± 0.10	16.55 ± 0.38	14.97 ± 0.23	2.24 ± 0.05	4.64 ± 0.17	3.94 ± 0.11	2.84 ± 0.22	2.40 ± 0.06	99.89
20	48.52 ± 0.79	2.93 ± 0.16	17.89 ± 0.41	7.42 ± 0.38	3.38 ± 0.60	5.69 ± 0.20	3.96 ± 0.15	2.60 ± 0.28	3.57 ± 0.09	98.92
21	48.37 ± 0.32	2.46 ± 0.13	19.62 ± 0.21	3.56 ± 0.13	3.83 ± 0.65	5.21 ± 0.28	5.38 ± 0.90	3.03 ± 0.16	3.27 ± 0.62	97.52
22	46.56 ± 0.80	3.69 ± 0.28	18.98 ± 0.48	0.02 ± 0.01	4.21 ± 1.92	8.13 ± 0.80	4.07 ± 0.50	2.10 ± 0.59	4.85 ± 0.01	98.01
23	49.69 ± 0.80	2.65 ± 0.06	18.08 ± 0.28	13.18 ± 0.07	2.76 ± 0.29	4.13 ± 0.08	4.35 ± 0.67	0.06 ± 0.01	3.05 ± 0.14	100.25
24	48.52 ± 1.59	2.74 ± 0.21	16.81 ± 0.84	12.52 ± 0.30	2.94 ± 0.35	4.38 ± 0.30	3.29 ± 0.78	1.52 ± 0.25	3.97 ± 0.20	101.30
25	43.35 ± 0.21	3.15 ± 0.12	13.79 ± 0.16	13.14 ± 0.38	3.32 ± 0.13	7.02 ± 0.09	3.22 ± 0.13	2.18 ± 0.16	–	90.54

etry (SIMS) analyses performed in reasonable integration times (≤200 s per peak). Niobium oxide (Nb_2O_5), metallic tantalum and lanthanum oxide (La_2O_3) were used as spikes for Nb, Ta and La at abundances of approximately 140, 700 and 70 ppm, respectively, and 20 wt% water was added to the starting material in order to promote amphibole crystallisation.

Experiments were done at the Mineralogisch-Petrologisches Institut of the University of Göttingen, in a 22-mm piston-cylinder apparatus (graphite furnace and CaF_2 as pressure media) by the hot-piston-out technique at a pressure of 1.4 GPa; no correction for friction was applied. Pt capsules were used, and oxygen fugacity was buffered using an inner graphite capsule to f_{O_2} conditions about 2 log units below FMQ. Temperature was measured with a $Pt–Pt_{90}Rh_{10}$ thermocouple, and its accuracy is estimated to be within ±10°C. The system was first brought to super-liquid conditions (T_{sl} = 1245–1255°C) for 1 h to homogenise the melt. It was then slowly cooled at a rate of 0.5–1°C/min to the equilibrium run temperature (T_{eq} = 850–1075°C) and kept at T_{eq} for 13 h. Quenching was obtained by switching the power off and the quenching rate was estimated to be around 900°C/min, meaning that subsolidus conditions were reached in a few seconds. A summary of the relevant parameters concerning charge compositions and synthesis conditions is reported in Table 1.

2.2. Chemical and structural characterisation

Major elements were analysed on polished mounts of the experimental charges with a JEOL JXA-840A electron microprobe (EMP) at the Centro Grandi Strumenti of the University of Pavia. Trace-element and H-, F- and Cl-contents of both glass and amphibole were determined by Cameca IMS 4f SIMS using analytical procedures developed at the CNR-CSCC [27,28]. Accuracy of Ti La, and H_2O data is 5, 10 and 15%, respectively, whereas that of Nb and Ta is estimated to

Table 5
Average Ti, Nb, Ta and La contents (in ppm) in amphiboles and glasses from SIMS analyses

Sample	Ti		Nb		Ta		La	
	Amph	Glass	Amph	Glass	Amph	Glass	Amph	Glass
1	28684 ± 503	13661 ± 176	20.1 ± 0.1	144 ± 2	–	–	11.5 ± 2.4	119 ± 0.1
2	33642 ± 1144	11759 ± 18	120 ± 11	233 ± 6	499 ± 28	1266 ± 51	25.5 ± 3.4	122 ± 1
3	24318 ± 1630	15541 ± 1238	51.0 ± 4.8	367 ± 53	161 ± 19	1401 ± 161	19.7 ± 3.9	231 ± 28
4	32435 ± 276	11931 ± 15	74.3 ± 4.1	205 ± 8	392 ± 8	1226 ± 85	15.5 ± 1.8	105 ± 2
5	31390 ± 2672	10814 ± 131	78.2 ± 8.5	227 ± 5	420 ± 23	1334 ± 60	20.5 ± 0.8	114 ± 1
6	33724 ± 1012	8975 ± 61	100 ± 0.1	224 ± 8	539 ± 8	1544 ± 5	27.2 ± 2.8	120 ± 0.1
7	26950 ± 919	6642 ± 32	135 ± 12	190 ± 7	565 ± 75	1167 ± 50	27.8 ± 4.2	105 ± 4
8	30949 ± 1334	6069	111 ± 27	97.4	–	–	30.9 ± 1.9	62.0
9	25569 ± 427	9044 ± 1217	150 ± 27	214 ± 13	594 ± 97	1217 ± 60	36.4 ± 2.7	153 ± 9
10	34148 ± 1048	13087 ± 582	114 ± 12	219 ± 32	524 ± 80	1254 ± 223	43.3 ± 8.1	144 ± 6
11	32898 ± 188	16637 ± 1343	87.3 ± 5.1	227 ± 12	396 ± 17	1180 ± 55	32.5 ± 1.9	148 ± 8
12	37204 ± 1496	17617 ± 419	91.0 ± 1.6	226 ± 2	417 ± 25	1143 ± 1	31.7 ± 3.7	137 ± 3
13	35830 ± 2600	15645 ± 590	104 ± 0.3	236 ± 13	450 ± 6	1264 ± 112	30.0 ± 2.9	117 ± 2
14	29772 ± 147	9427 ± 147	141 ± 4	234 ± 4	568 ± 10	1387 ± 10	46.7 ± 2.5	135 ± 2
15	33604 ± 2860	14585 ± 443	90.9 ± 17.1	232 ± 22	401 ± 83	1226 ± 174	26.2 ± 5.8	137 ± 10
16	19621 ± 26	33831 ± 23	8.56 ± 0.4	137 ± 2	44.2 ± 2	713 ± 6	3.95 ± 0.04	69.7 ± 0.1
17	20548 ± 604	2521 ± 17	319 ± 14	196 ± 13	1283 ± 86	1286 ± 111	38.1 ± 0.6	154 ± 5
18	24106 ± 1219	4432 ± 200	151 ± 5	218 ± 13	716 ± 62	1318 ± 57	35.4 ± 10.6	131 ± 5
19	35652 ± 666	14806 ± 103	99.7 ± 17.3	214 ± 7	449 ± 36	1246 ± 53	25.2 ± 0.4	119 ± 2
20	38794 ± 2115	18071 ± 539	71.3 ± 4.1	268 ± 3	367 ± 35	1298 ± 32	28.0 ± 0.7	155 ± 4
21	33796 ± 2008	16333 ± 823	67.5 ± 7.9	387 ± 39	375 ± 38	1622 ± 185	31.4 ± 1.1	178 ± 21
22	29810 ± 1025	24868 ± 4108	46.9 ± 7.9	369 ± 10	271 ± 40	1508 ± 63	23.8 ± 1.6	170 ± 24
23	33948 ± 692	17707 ± 298	96.6 ± 20.7	256 ± 1	409 ± 15	1206 ± 27	24.1 ± 0.1	154 ± 3
24	31944 ± 242	17961 ± 1318	68.1 ± 3.9	236 ± 5	295 ± 2	1190 ± 7	22.4 ± 0.1	135 ± 1
25	23064 ± 778	20078 ± 237	51.9 ± 3.8	287 ± 2	250 ± 20	1505 ± 26	15.3 ± 1.0	131 ± 2

Standard deviations are calculated considering at least two different points within each experimental charge.

be about 15% for Nb and 25% for Ta. Systematic errors in the calibration of ion currents versus concentrations are cancelled when calculating the partition coefficients (D), and matrix effects are small because of the narrow compositional difference between amphibole and glass. Thus the accuracy of D is estimated in the order of a few percent for all three elements.

Amphibole single-crystals of dimensions suitable for structure refinements (SREF, for details on the adopted procedures the reader is referred to [29]) were obtained in nearly all experimental runs. Selected results relevant to the present discussion are reported in Table 2; further details can be obtained from the authors upon request. The refined crystals were subsequently embedded in epoxy resins, polished and analysed for major and trace element as well as for H, Cl and F.

The combination of EMP and SREF results shows complete A-site occupancy for all the selected crystals except sample 16. Unit formulas were calculated on the basis of 24 (O, OH, F) and changing the Fe^{2+}/Fe^{3+} ratio to obtain the correct number of cations. The amounts of oxy-component ($^{O3}O^{2-}$) were confirmed by diagnostic SREF results [30,31]. Group-site populations and octahedral site-populations were obtained by minimising the differences between the refined site-scatterings and mean bond-lengths and those calculated from the unit formulas (Table 3). $^{O3}O^{2-}$ is balanced mainly by $^{M1}Ti^{4+}$, with sporadic contributions from subordinate amounts of $^{M1,3}Fe^{3+}$.

3. Results

The run products are amphibole as the dominant crystalline phase (plus subordinate olivine and clinopyroxene) and glass. Chemical data for amphibole and glass are reported in Tables 3–6.

Table 6
Amphibole/melt partition coefficients for Ti_{Tot}, Ti_{M1}, Ti_{M2}, Nb, Ta, La and Nb/Ta and Nb/La ratios

Sample	Ti_{Tot}	^{M2}Ti	^{M1}Ti	Nb	Ta	La	Nb/Ta	Nb/La
1	2.08 ± 0.05	0.541	1.540	0.138 ± 0.002	–	0.10 ± 0.02	–	1.42 ± 0.30
2	2.86 ± 0.10	0.744	2.117	0.51 ± 0.05	0.39 ± 0.03	0.21 ± 0.03	1.30 ± 0.15	2.47 ± 0.40
3	1.57 ± 0.16	0.297	1.268	0.14 ± 0.02	0.12 ± 0.02	0.09 ± 0.02	1.21 ± 0.29	1.64 ± 0.47
4	2.72 ± 0.02	0.598	2.120	0.36 ± 0.03	0.32 ± 0.02	0.15 ± 0.02	1.13 ± 0.11	2.46 ± 0.33
5	2.90 ± 0.25	0.813	2.091	0.34 ± 0.04	0.32 ± 0.02	0.18 ± 0.01	1.09 ± 0.14	1.91 ± 0.23
6	3.76 ± 0.12	0.789	2.969	0.45 ± 0.02	0.35 ± 0.01	0.23 ± 0.02	1.28 ± 0.05	1.98 ± 0.22
7	4.06 ± 0.14	1.095	2.962	0.71 ± 0.07	0.48 ± 0.07	0.26 ± 0.04	1.47 ± 0.25	2.67 ± 0.49
8	5.10	1.377	3.723	1.14	—	0.50	—	2.28
9	2.86 ± 0.39	0.458	2.402	0.70 ± 0.13	0.49 ± 0.08	0.24 ± 0.02	1.44 ± 0.37	2.93 ± 0.62
10	2.61 ± 0.14	0.601	2.013	0.52 ± 0.09	0.42 ± 0.10	0.30 ± 0.06	1.25 ± 0.37	1.75 ± 0.46
11	1.99 ± 0.16	0.476	1.509	0.39 ± 0.03	0.34 ± 0.02	0.22 ± 0.02	1.15 ± 0.12	1.76 ± 0.20
12	2.11 ± 0.10	0.507	1.605	0.40 ± 0.01	0.36 ± 0.02	0.23 ± 0.03	1.10 ± 0.07	1.74 ± 0.21
13	2.29 ± 0.19	0.320	1.968	0.44 ± 0.02	0.36 ± 0.03	0.26 ± 0.03	1.23 ± 0.13	1.71 ± 0.19
14	3.16 ± 0.05	0.442	2.716	0.60 ± 0.02	0.41 ± 0.01	0.35 ± 0.02	1.48 ± 0.06	1.74 ± 0.12
15	2.30 ± 0.01	0.368	1.934	0.39 ± 0.08	0.33 ± 0.08	0.19 ± 0.04	1.20 ± 0.39	2.06 ± 0.64
16	0.580 ± 0.001	0.418	0.162	0.062 ± 0.003	0.062 ± 0.003	0.057 ± 0.001	1.01 ± 0.06	1.10 ± 0.05
17	8.15 ± 0.25	1.793	6.357	1.63 ± 0.13	1.00 ± 0.11	0.25 ± 0.01	1.63 ± 0.22	6.60 ± 0.57
18	5.45 ± 0.37	1.582	3.873	0.69 ± 0.05	0.54 ± 0.05	0.27 ± 0.08	1.27 ± 0.15	2.58 ± 0.80
19	2.41 ± 0.05	0.385	2.023	0.47 ± 0.08	0.36 ± 0.03	0.212 ± 0.005	1.29 ± 0.26	2.21 ± 0.39
20	2.15 ± 0.13	0.774	1.376	0.27 ± 0.02	0.28 ± 0.03	0.18 ± 0.01	0.94 ± 0.11	1.47 ± 0.10
21	2.07 ± 0.16	0.766	1.304	0.17 ± 0.03	0.23 ± 0.04	0.18 ± 0.02	0.75 ± 0.16	0.99 ± 0.20
22	1.21 ± 0.20	0.606	0.606	0.13 ± 0.02	0.18 ± 0.03	0.14 ± 0.02	0.71 ± 0.16	0.91 ± 0.21
23	1.92 ± 0.05	0.652	1.266	0.38 ± 0.08	0.34 ± 0.01	0.157 ± 0.003	1.11 ± 0.24	2.40 ± 0.52
24	1.78 ± 0.13	0.499	1.284	0.29 ± 0.02	0.248 ± 0.002	0.166 ± 0.001	1.16 ± 0.07	1.74 ± 0.11
25	1.15 ± 0.04	0.218	0.930	0.18 ± 0.01	0.17 ± 0.01	0.12 ± 0.01	1.09 ± 0.12	1.55 ± 0.15

Values are averaged in all experiments. The $^{Amph/L}D$ for ^{M1}Ti and ^{M2}Ti were calculated by multiplying the $^{Amph/L}D_{TiTot}$ for the ratios $Ti_{Tot}/\ ^{M1}Ti$ and $Ti_{Tot}/\ ^{M2}Ti$, respectively.

The degree of crystallisation is less than 50% in all experiments, and no quench crystals were found in the glass. Textural relations between minerals indicate that amphibole is the last phase in the crystallisation sequence. The absence of significant major-element zoning in both amphibole and glass, as determined by EMP traverses, and the euhedral habitus of the amphibole crystals (Fig. 1) indicate conditions close to equilibrium. The low standard deviations (S.D.) obtained for major and trace elements (Tables 3–5) indicate that both amphibole and glass are essentially homogeneous within single experimental charges.

Amphiboles are titanian pargasite and kaersutite according to the nomenclature scheme in force [32], and are characterised by $^{[4]}Al$ contents around two atoms per formula unit (apfu) and by $^{O3}O^{2-}$contents ranging between 0.61 and 1.11 apfu (Table 3). The Mg/(Mg+Fe*) ratio (*mg*#) and the Na/(Na+K) ratio (*na*#) closely resemble those of the starting material, and range from 0.36 to 1.0, and from 0.67 to 1, respectively. In one case (sample 16), a higher F content was added to the mixture, and caused the crystallisation of a F-rich (0.75 apfu), poorly dehydrogenated ($^{O3}O^{2-} = 0.24$ apfu) pargasite. Dehydrogenation is a common feature of upper-mantle and magmatic amphiboles because: (1) it enhances the stability of the amphibole structure at high T avoiding the need for the weak O3–H bonds; (2) it allows amphibole crystallisation at low f_{H_2O} conditions. The values of dehydrogenation obtained in this set of experiments are similar to those reported in previous work of the CSCC [33,34] for naturally occurring mantle amphiboles.

The glasses range from picrobasalt through trachyandesite to trachyite (Table 4), and the *mg*# (0.08–1) of the glass reflects that of the starting material. Analysed H_2O contents are between 2.4 and 6.1 wt%. The concentrations of Nb, Ta and

La are all below 1700 ppm (Table 5), and no deviation from the Henry's law behaviour is expected at such concentrations [35].

Two to four sets of amphibole/liquid partition coefficients were calculated for each experimental charge from analyses of adjacent points in amphibole and glass. Table 6 lists the average $^{Amph/L}D$s for Nb, Ta and La together with their standard deviations.

$^{Amph/L}D_{Nb}$ ranges from 0.14 to 1.63, and $^{Amph/L}D_{Ta}$ from 0.12 to 1.00. In the F-rich amphibole (sample 16) $^{Amph/L}D_{Nb,Ta}$ are much lower and both equal to 0.06. $^{Amph/L}D_{Nb}$ and $^{Amph/L}D_{Ta}$ are strongly correlated (Fig. 2), but the $^{Amph/L}D_{Nb/Ta}$ ratio exhibit a wide range (from 0.71–1.63). $^{Amph/L}D_{La}$ ranges from 0.09 to 0.50 in F-poor partially dehydrogenated amphiboles, but is only 0.06 in the F-rich amphibole. The D_{Nb}/D_{La} ratio is also highly variable (0.91–6.60). This new set of $^{Amph/L}D_{Nb}$ and $^{Amph/L}D_{Ta}$ encompasses the whole range so far reported in the literature [21–23,36–38] (Fig. 2).

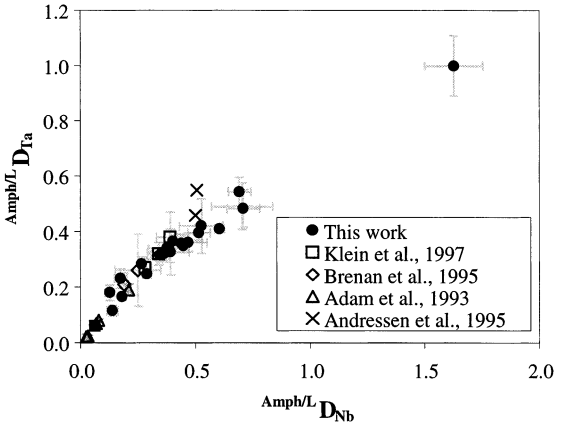

Fig. 2. $^{Amph/L}D_{Nb}$ and $^{Amph/L}D_{Ta}$ for the samples of this work (filled symbols) and for the data available in the literature (open symbols and cross). The filled square refers to the F-rich sample.

4. Discussion

4.1. Site preference of Nb and Ta in titanian pargasite and kaersutite

On the basis of their valence and ionic radius (0.64 Å [39] is commonly used for both elements in six-fold co-ordination), Nb and Ta are expected to be incorporated into one or more of the three independent octahedral sites of the amphibole structure (namely, M1, M2 and M3). Due to the very low concentrations, their site preference cannot be detected directly by SREF; it can neither be inferred by comparing the refined geometrical parameters with those obtained by modelling on the basis of the elastic-strain theory [40], because this procedure requires at least three homovalent substituents at the same site.

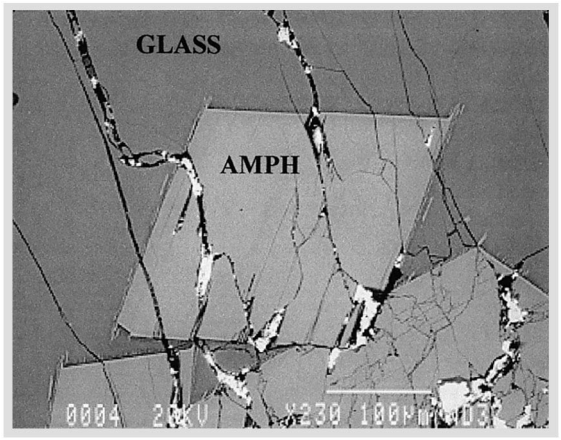

Fig. 1. Back-scattered image of an amphibole grain in sample 1, showing regular crystal morphology and a clean well-quenched glass.

Information about Nb and Ta site preference in titanian pargasite and kaersutite can be derived by considering partition coefficients between amphibole and clinopyroxene ($^{Amph/Cpx}D$). Whereas couples of sites are crystal-chemically analogous in the two mineral structures ($M1_{Cpx} \leftrightarrow M2_{Amph}$, $M2_{Cpx} \leftrightarrow M4_{Amph}$), some other sites (and thus some substitution mechanisms) are specific to amphibole, and do not occur in clinopyroxene. If we compare $^{Amph/Cpx}D$s calculated for selected trace-elements for run no. 2 (Fig. 3), in which equilibrium conditions are well documented by chemical homogeneity and euhedral texture of coexisting crystals, we see that REE, Y, Hf and Zr have $^{Amph/Cpx}D$ values around 3–5, whereas Ba, K, Nb and Ta have $^{Amph/Cpx}D$ one to two orders of magnitude higher (Fig. 3). Noticeably, these re-

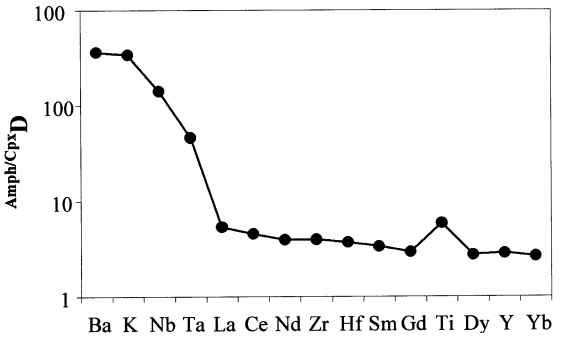

Fig. 3. Selected trace-element partition coefficients between amphibole and clinopyroxene from sample 2. Nb and Ta abundances are much higher in amphibole, indicating incorporation into non-analogous sites in the two minerals.

sults are consistent with similar findings from studies of natural clinopyroxene/amphibole pairs from mantle xenoliths and peridotite massifs [34], thus providing an important evidence to solve apparent inconsistency between Amph/Cpx partitioning of Nb and Ta obtained for natural and experimental systems [41]. These distinct features can be explained by assuming that the first set of elements is incorporated into analogous sites according to the same crystal–chemical mechanisms, and hence have a similar compatibility in the two minerals, whereas the second set is incorporated according to mechanisms which are present solely in amphibole. REE are mainly incorporated in the analogous $M2_{Cpx}$ and $M4_{Amph}$ sites in pargasite [42], and Zr and Hf enter the analogous $M1_{Cpx}$ and $M2_{Amph}$ in calcic amphibole together with the fraction of Ti which is involved in the local balance of tetrahedral Al [40].

The high values of the $^{Amph/Cpx}D$ observed for Ba and K are due to the presence of the 12-fold co-ordinated A site in the amphibole structure; those for Nb and Ta also require that these elements participate in crystal–chemical mechanisms involving octahedral sites, which are not possible in clinopyroxene. The only significant difference in the crystal-chemistry of the octahedral sites in the two mineral phases is the presence of the O3 site in amphibole, which may be occupied by monovalent anions (OH, F, Cl), but also by O^{2-} (after dehydrogenation). Dehydrogenation causes dramatic changes in the local charge-distribution, and charge balancing is accomplished mainly by the incorporation of $^{M1}Ti^{4+}$ and/or $^{M1,M3}Fe^{3+}$ (cf. [31] for further details on Ti distribution and on dehydrogenation in amphibole). Given the significant dehydrogenation observed in the high-T calcic amphiboles of this study, Ti^{4+} is mainly ordered at M1, with only subordinate and negligible amounts at M2 and M3, respectively (Table 3). Qualitative information about the site preference of Nb and Ta can be obtained by comparing $^{Amph/L}D_{Nb,Ta}$ with site-specific partition coefficients for titanium, namely those calculated by considering only the fraction of Ti in a specific site. In the following, we refer to these site-specific partition coefficients using the notation $^{Amph/L}D_{M1Ti}$ and $^{Amph/L}D_{M2Ti}$. Fig. 4 shows that $^{Amph/L}D_{Nb}$ significantly correlates to $^{Amph/L}D_{M1Ti}$, and very poorly to $^{Amph/L}D_{M2Ti}$, especially at low values of $^{Amph/L}D_{Nb}$; the same behaviour is observed for $^{Amph/L}D_{Ta}$. These trends are consistent with predominant Nb and Ta incorporation into M1. Thus Nb and Ta participate

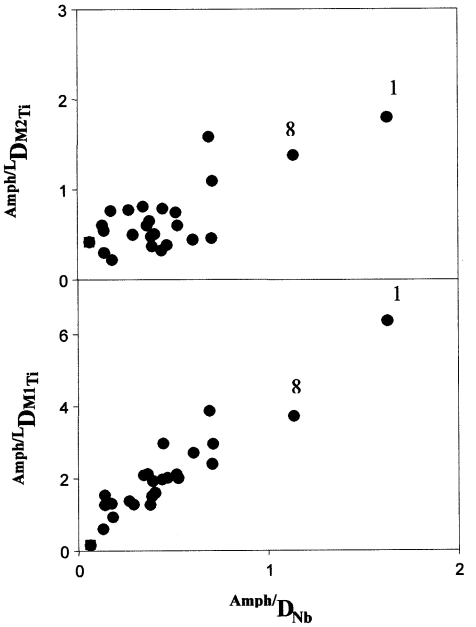

Fig. 4. The relation between $^{Amph/L}D_{Nb}$ and the site-specific partial partition coefficients for Ti. The good correlation with ^{M1}Ti indicates preferential Nb incorporation into M1, and involvement in the balancing of dehydrogenation. The filled square refers to the F-rich sample.

actively in the local charge-balance of dehydrogenation, providing three additional positive charges (with respect to Mg and Fe^{2+}) without causing significant shrinking of the octahedral site and consequent deformation of the octahedral strip.

In the case of amphibole with scarce or null oxy-component, Nb and Ta are expected to be incorporated into the M2 site, together with the other high-charge cations (e.g., Hf and Zr) in order to balance the presence of $^{[4]}$Al. Obviously, it cannot be excluded that this mechanism is partially active also in dehydrogenated amphiboles (and in particular in samples 8 and 17, where some correlation with $^{Amph/L}D_{TiM2}$ is apparent), but it is most likely subordinated as suggested by the very low D observed in clinopyroxene and in sample 16, which has $^{O3}O^{2-} = 0.24$ apfu.

4.2. Factors affecting Nb and Ta incorporation in amphiboles

Mineral/liquid partition coefficients are dependent on the composition and the structure of both melt and crystal. The effect of melt polymerisation on $^{Amph/L}D$ is related to both the ionic charge and the ionic radius of the elements [43], and hence is expected to severely affect the compatibility of pentavalent cations. Owing to the lack of knowledge of Fe^{3+}/Fe^{2+} ratio and of H speciation in the melt, which are needed to correctly calculate the NBO/T ratio, we tried a comparison simply on the basis of the silica content. Fig. 5 shows that $^{Amph/L}D$ values for Nb and Ta increase more than six times in the observed SiO_2 range of the melt (41.5–54.6 wt%). At high SiO_2 contents, two samples (8 and 17) diverge from the main trend to $^{Amph/L}D_{Nb}$ values above unity. These samples represent Ti-depleted systems, in which $^{Amph/L}D_{M1Ti}$, as well as the D of all high-charge cations, increase to allow incorporation of sufficient Ti to balance dehydrogenation. Dehydrogenation is the main factor controlling $^{Amph/L}D$ for Nb and Ta. In the only two amphiboles crystallised in equilibrium with liquids with similar SiO_2 content (16 and 25; $SiO_2 = 41.5$ wt% and 43.3 wt%) a three-fold increase in the oxy-component (from 0.24 to 0.76 apfu) causes a threefold variation in

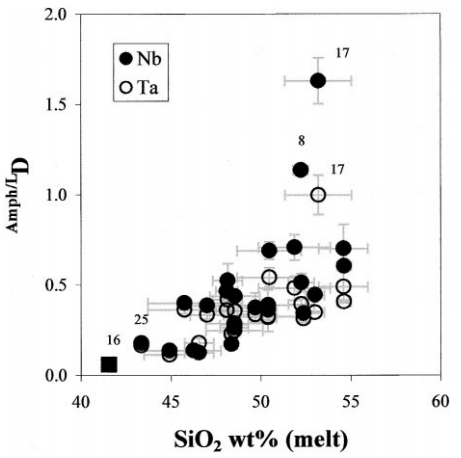

Fig. 5. $^{Amph/L}D_{Nb}$, $^{Amph/L}D_{Ta}$ and the SiO_2 content of the melt. The samples deviating from the main trend are from Ti-depleted systems (runs 8 and 17). Numbers are sample codes referring to experiments in Table 1.

$^{Amph/L}D_{Nb,Ta}$ (from 0.062 to 0.181). The very low values for $^{Amph/L}D_{Nb}$ reported in [21] for F-rich amphiboles with low oxy-component also confirm this evidence.

4.3. Factors affecting Nb/Ta fractionation in amphiboles

$^{Amph/L}D_{Nb/Ta}$ values range from 0.71 to 1.63 in the amphiboles of this work; they should be close to 1 if the ionic radii of Nb and Ta were both equal to 0.64 Å, as it is commonly assumed [39]. Fractionation of elements between mineral and melt or between couples of mineral phases is due either to their ionic charges or their ionic radii. Cations with different charges may be involved in different crystal–chemical substitution mechanisms or in the same mechanism but in different extents, and may also be fractionated by the melt structure [43]. Cations with the same charge may be discriminated on the basis of their ionic radius by the crystal structure, i.e., by the size and the compliance of the relevant sites.

No direct method is available to unambiguously verify the actual valence of Nb and Ta in these complex compositions, however, the correlation of $^{Amph/L}D_{Nb/Ta}$ with the dimension of the

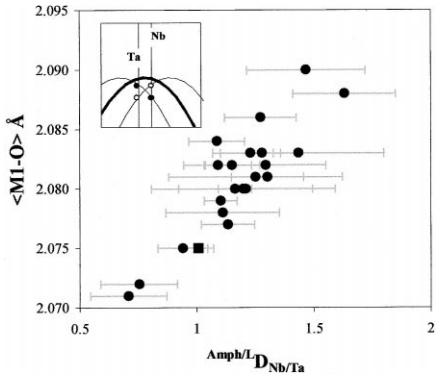

Fig. 6. The relation between $^{Amph/L}D_{Nb/Ta}$ and the dimension of the M1 site. The preference for Ta and Nb incorporation inverts at around 2.077 Å. The inset schematically shows a model for Nb,Ta fractionation as a function of the site dimension assuming an ionic radius of Nb greater than that of Ta. The filled square refers to the F-rich sample.

M1 site and the inversion in the preference at ⟨M1−O⟩ around 2.077 Å (Fig. 6) are most likely related to a difference in the ionic radii. We can explain this inversion if Nb and Ta lie close to the apex of an Onuma curve (Fig. 6, inset). In the frame of the elastic-strain theory [44] the inversion point of 0.697 Å (2.077 Å−1.38 Å, where 1.38 Å is the ionic radius of $^{[4]}O^{2-}$ [39]) corresponds approximately to the average of the two ionic radii. The higher compatibility of Nb at longer ⟨M1−O⟩ implies that Nb is larger than Ta. Given the ranges of variations observed for ⟨M1−O⟩ (2.071–2.090 Å) and for $^{Amph/L}D_{Nb/Ta}$ (0.71–1.63), and fixing the temperature at 1000°C, we can derive the difference between the ionic radii of Nb and Ta as a function of the Young's modulus (E) and of the ideal-cation radius of the site (equation # 3 in [44]). We assumed E values in the range 5000–4000 GPa, slightly higher than those calculated for tetravalent elements at the M2 site for the same amphiboles [40], and obtained a difference between the ionic radii of Nb and Ta in the range 0.01–0.02 Å. Noticeably, it is close to that reported for the twin elements Zr and Hf, that also similarly differ in their electronic configuration.

The large discrepancy between the average of the ionic radii from Fig. 6 (0.697 Å) and the tabulated ionic radii of 0.64 Å [39] can be explained by the high Ti contents at M1. Ti orders at an off-centre position (M1′) shifted towards the O3–O3 edge, with more distorted co-ordination and shorter cation-oxygen distances than those of the central position ([40], and references therein). Nb and Ta are also likely to order at an off-centre position, more suitable for providing the maximum bond valence on the O3 oxygens where dehydrogenation occurs. Thus the local mean bond-length would be shorter than the long-range averaged value obtained by SREF. Noticeably, the ionic radii of Nb and Ta may increase with site distortion [39].

5. Applications

5.1. The prediction of the $^{Amph/L}D_{Nb/Ta}$ in natural systems

We have shown that $^{Amph/L}D_{Nb/Ta}$ values are related to the ∠M1–O⟩ distance in the titanian pargasites and kaersutites of the present work. ⟨M1−O⟩ can be measured only by structure refinement, which is not of common use in petrological studies; we provide here a simplified model to predict Nb/Ta fractionation in amphiboles that can be applied on major-element composition determined by the electron probe.

In dehydrogenated titanian pargasite and kaersutite, ⟨M1−O⟩ depends on $^{M1}mg\#$, ^{M1}Ti, $^{M1}Fe^{3+}$ and F content, so that all these parameters are in principle needed to predict site dimension. However, some simplifying assumptions can be done: (1) the $mg\#$ at M1 can be reasonably approximated to a constant proportion of the bulk $mg\#$, as comparative crystal–chemical studies at CSCC have shown that the M1 and M3 sites do not fractionate Mg and Fe^{2+} at high temperatures (>900°C); (2) the amount of Ti at the M1 site is a nearly constant fraction (∼70–80%) of the total Ti in dehydrogenated titanian pargasite and kaersutite; (3) Fe^{3+} at M1 is rare in amphiboles where dehydrogenation was present since crystallisation, and the F contents are low in mantle amphiboles.

Scaling by a constant value does not affect the slope of a relation, and thus the reliability of our

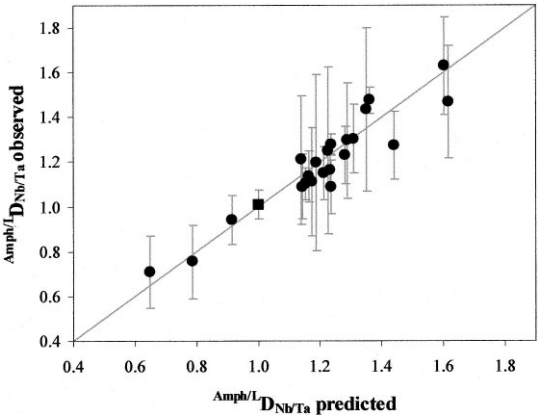

Fig. 7. The comparison between observed $^{Amph/L}D_{Nb/Ta}$ and those calculated according to Eq. 2. The filled square refers to the F-rich sample.

predictive model. The regression equation relating the total *mg*# and Ti contents to ⟨M1−O⟩:

$$\langle M1-O\rangle = 2.10-0.023\ mg\#-0.014\ Ti_{Tot} \quad (R^2 = 0.83) \qquad (1)$$

has an average error in the estimate of ⟨M1−O⟩ around 0.003 Å.

The dependence of $^{Amph/L}D_{Nb/Ta}$ on the site dimension has an exponential form, but the difference with linear dependence is smaller than the spread in the data; given the reasonable correlation factor in Eq. 1, we expressed ⟨M1−O⟩ in terms of *mg*# and Ti_{Tot} and calculated the following linear regression equation, in which the data were weighted according to $1/\sigma^2$:

$$^{Amph/L}D_{Nb/Ta} = 2.45-1.26\ mg\#-0.84\ Ti_{Tot} \quad (R^2 = 0.84) \qquad (2)$$

A plot of predicted vs. observed values is shown in Fig. 7. The average error of the predicted values in our data set is 7%, and the maximum error (for sample 21) is 20%. The application of this equation to amphiboles should be restricted to titanian pargasites and kaersutites with a significant oxy-component and crystallised at similar temperature and pressure. Significant changes in the crystal chemistry of amphibole (particularly in $^{[4]}$Al or in dehydrogenation) may either invalidate the assumptions underlying Eq. 1, or imply different crystal–chemical mechanisms for the incorporation of Nb and Ta. Data from previous studies on Nb and Ta partitioning in hornblende were not included in the formulation of this model.

5.2. Constraints on the fractionation of Nb relative to REE

The fractionation of Nb and Ta from trace elements of nominally similar incompatibility is also of considerable geochemical interest. The differing valencies and site preferences of Nb (and Ta) with respect to the light rare earth elements (LREE) preclude the development of a quantitative predictive model on the basis of the current data set. Nevertheless, some qualitative considerations can constrain the behaviour of Nb and Ta relative to other incompatible elements during mineral/melt processes involving titanian pargasite and kaersutite. We have shown that high $^{Amph/L}D_{Nb,Ta}$ values may occur only in amphiboles with significant oxy-component ($O^{2-} > 0.6$ apfu), and that at constant oxy-component $^{Amph/L}D_{Nb,Ta}$ values depend on the SiO_2 and TiO_2 contents of the melt. Both these factors affect the fractionation of the $^{Amph/L}D$ of Nb relative to those of the other incompatible elements. The higher charge of Nb makes it less compatible to the melt than REE with increasing SiO_2.

The Ti content of the melt affects the degree of dehydrogenation of the amphiboles through f_{O_2} and f_{H_2O}, but does not affect $^{Amph/L}D_{REE}$; thus it further fractionates the Nb/REE ratio. If we consider a differentiation process from a basanite or an alkali basalt driven mainly by fractional crystallisation of an amphibole-dominated assemblage, the residual melts will be depleted in TiO_2 and MgO and enriched in SiO_2 as crystallisation proceeds. The chemical evolution of the melt is approximated by the *mg*# of the amphibole, which is related to that of the melt [23]. The $^{Amph/L}D_{Nb/La}$ values correlate negatively with *mg*# (Fig. 8), and thus positively with the degree

of crystal fractionation. At high values of *mg#* (0.9) there is little or no fractionation of Nb from La, whereas Nb is three times more compatible than La at *mg#* of about 0.4. This behaviour is partly a consequence of Ti-depletion in the melt, a prerequisite for attaining the highest values of $^{Amph/L}D_{Nb/La}$. Unfortunately, our experimental data-set does not include results for high-*mg#* and Ti-poor systems, and therefore is not able to unravel the competing effects of TiO_2 and SiO_2 on partition coefficients. However it is expected that the Ti content of the melt exerts a strong control on $^{Amph/L}D_{Nb}$ also at high *mg#* due to the need of incorporating high-charge cations to increase the amphibole stability.

5.3. Implications for trace-element control by melting and crystallisation in natural systems

The above model for Nb/Ta and Nb/La fractionation can be rigorously applied only to the amphibole compositional range of this work ($^{[4]}Al = 1.9–2.2$ apfu; $Ti > 0.34$ apfu; $O^{2-} = 0.61–1.11$ apfu), as distinct incorporation mechanisms for high-field strength elements may be active under other conditions; however, this compositional range includes amphiboles with significant amounts of dehydrogenation crystallised at high pressures and temperatures, and thus the model should apply to mantle peridotites and amphibolites under conditions of partial melting. Both these amphibole-bearing parageneses are relevant to magma genesis in subduction zones, and are probably important for the generation of convergent margin igneous rocks and of the bulk continental crust.

The main difference between amphibole peridotite and amphibolite with regard to the predictive model for Nb/Ta and Nb/La fractionation concerns *mg#*. In amphibole peridotite the *mg#* is buffered at close to 0.9 by the other silicate minerals [45]; for these pargasite compositions, the Nb/La ratio should be approximately 1 or even lower (Fig. 8). This suggests that amphiboles in equilibrium with mantle peridotite cannot generate negative anomalies for Nb and Ta, nor low Nb/Ta ratios in coexisting melts. Accordingly, exceptionally high Nb and Ta concentrations have

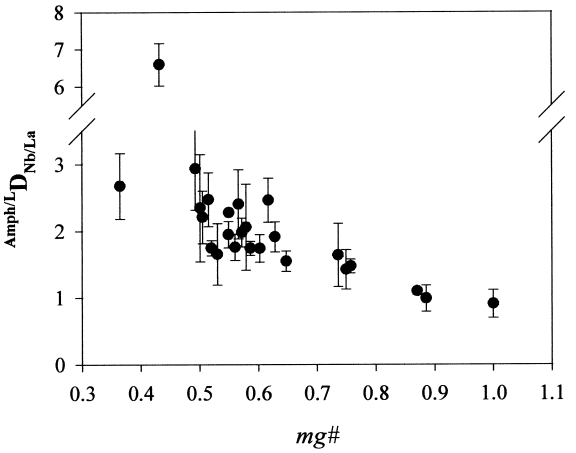

Fig. 8. The relation between $^{Amph/L}D_{Nb/La}$ and *mg#*. Numbers are sample codes referring to experiments in Table 1. Fractionation of Nb from LREE due to amphibole crystallisation or melting should only occur where the *mg#* is relatively low.

been commonly documented in vein amphiboles relative to amphiboles disseminated through the peridotite, in keeping with the findings in nearby [46] and other [34] areas. Thus, although amphibole peridotite does not appear to be a major controlling factor on the Nb–Ta budget of convergent margin magmas, particularly in view of the low modal abundance of amphibole, it may play a role for vein parageneses [47]. The considerations reported above hold in the case of amphibole/silicate-melt equilibrium. It is plausible that the interaction of a silica-rich aqueous fluid with ambient peridotite may also lead to the crystallisation of disseminated low-*mg#* amphiboles capable to significantly fractionate Nb.

Partial melting of amphibolites is not thought to be a major factor in present-day subduction-zone magma genesis, being limited to the production of adakitic magmas in areas of anomalously high geothermal gradient [48,49]. However, these conditions may have been much more common in the late Archean corresponding to a major growth episode of continental crust. The generally lower *mg#* of amphiboles (0.5–0.6) in amphibolites undergoing melting should lead to high $^{Amph/L}D_{Nb/Ta}$ and $^{Amph/L}D_{Nb/La}$ values, and their high modal abundance enables production of a

low Nb/Ta and low Nb/La signature in coexisting melts. Amphibole in the subducting slab during melting thus appears to be a possible explanation for negative Nb–Ta anomalies and low Nb/Ta ratios in melts, whereas amphibole disseminated throughout peridotite in the mantle wedge does not.

Amphibole may also occur as a phenocryst phase early in the fractionation series of water-rich convergent margin volcanics. The relations derived from our experimental data indicate that Nb is not expected to fractionate from La, at least until high degrees of fractionation and SiO_2-rich melt compositions are achieved. Low TiO_2 contents in these residual melts will enhance the resultant Nb–Ta anomalies.

Acknowledgements

This paper greatly benefited from constructive comments by Klaus-Peter Jochum, Dimitri Ionov and Mary R. Reid. Funding for this work was provided by the Consiglio Nazionale delle Ricerche to the CSCC and to Massimo Tiepolo (research grant), by the Ministero della Università e della Ricerca Scientifica e Tecnologica (project 'Transformations in subducted materials and mass transfer to the mantle wedge') to Riccardo Vannucci, and by the Deutsche Forschungsgemeinschaft (Grant Fo 181/9-1) to Steve Foley. *[AH]*

References

[1] A. Hofmann, K. Jochum, M. Seufert, W. White, Nb and Pb in oceanic basalts: new constraints on mantle evolution, Earth Planet. Sci. Lett. 79 (1986) 33–45.

[2] S.-S. Sun, W. McDonough, Chemical and isotopic systematics of ocean basalts: implications for mantle composition and processes, in: A.D. Saunders, M.J. Norry (Eds.), Magmatism in the Ocean Basins, Geol. Soc. London, Spec. Publ. 42 (1989) 313–345.

[3] J. Pearce, D. Peate, Tectonic implications of the composition of volcanic arc magmas, Annu. Rev. Earth Planet. Sci. 23 (1995) 251–285.

[4] R. Rudnick, D. Fountain, Nature and composition of the continental crust: a lower crustal perspective, Rev. Geophys. 33 (1995) 267–309.

[5] K.P. Jochum, A.W. Hofmann, A.J. Stolz, Low Nb/Ta in OIB Mantle, Terra Nova 9 Abstr. Suppl. 1, EUG 9, Strasbourg, (1997) 48.

[6] K.P. Jochum, H.M. Seufert, B. Spettel, H. Palme, The solar system abundances of Nb, Ta and Y, and the relative abundances of refractory lithophile elements in differentiated planetary bodies, Geochim. Cosmochim. Acta 50 (1986) 1173–1183.

[7] T. Plank, C.H. Langmuir, The chemical composition of subducting sediment and its consequences for the crust and mantle, in: F. Albarede, T.J. Blichert, H. Staudigel and W.M. White (Eds.), Geochemical Earth Reference Model (GERM), Elsevier 145, Amsterdam (1998) 325–394.

[8] A. Stolz, K. Jochum, B. Spettel, A. Hofmann, Fluid- and melt-related enrichment in the subarc mantle evidence from Nb/Ta variations in island arc basalts, Geology 24 (1996) 587–590.

[9] A. Duncan, The Karoo igneous province - a problem area for inferring tectonic setting from basalt geochemistry, J. Volcanol. Geotherm. Res. 32 (1987) 13–34.

[10] J. Marsh, Basalt geochemistry and tectonic discrimination within continental flood basalt provinces, J. Volcanol. Geotherm. Res. 32 (1987) 35–49.

[11] E. Klein, J. Karsten, Ocean–ridge basalts with convergent-margin geochemical affinities from the Chile Ridge, Nature 374 (1995) 52–57.

[12] Y. Niu, R. Batiza, Trace element evidence from seamounts for recycled oceanic crust in the East Pacific mantle, Earth Planet. Sci. Lett. 148 (1997) 471–483.

[13] J. Brenan, H. Shaw, D. Phinney, F. Ryerson, Rutile-aqueous fluid partitioning of Nb, Ta, Hf, Zr, U and Th: implications for high field strength element depletions in island-arc basalts, Earth Planet. Sci. Lett. 128 (1994) 327–339.

[14] J.C. Ayers, S.K. Dittmer, G.D. Layne, Partitioning of elements between peridotite and H_2O at 2.0–3.0 GPa and 900–1100 °C, and application to models of subduction zone processes, Earth Planet. Sci. Lett. 150 (1997) 381–398.

[15] R. Stalder, S.F. Foley, G.P. Brey, I. Horn, Mineral-aqueous fluid partitioning of trace elements at 900–1200°C and 3.0–5.7 GPa: new experimental data for garnet, clinopyroxene, and rutile, and implications for mantle metasomatism, Geochim. Cosmochim. Acta 62 (1998) 1781–1801.

[16] S. Foley, M. Barth, G. Jenner, Rutile/mlt partition coefficients for trace elements and an assessment of the influence of rutile on the trace element characteristics of subduction zone magmas, Geochim. Cosmochim. Acta (1999) submitted.

[17] J. Ayers, Trace element modeling of aqueous fluid- peridotite interaction in the mantle wedge of subduction zones, Contrib. Mineral. Petrol. 132 (1998) 390–404.

[18] D. Green, A. Ringwood, An experimental investigation of the gabbro to eclogite transformation and its petrological applications, Geochim. Cosmochim. Acta 31 (1967) 767–833.

[19] F.J. Ryerson, E.B. Watson, Rutile saturation in magmas: implications for Ti–Nb–Ta depletion in island-arc basalts, Earth Planet. Sci. Lett. 86 (1987) 225–239.
[20] D.A. Ionov, A.W. Hofmann, Nb–Ta-rich mantle amphiboles and micas: Implications for subduction-related metasomatic trace element fractionations, Earth Planet. Sci. Lett. 131 (1995) 341–356.
[21] J. Adam, T.H. Green, S.H. Sie, Proton microprobe determined partitioning of Rb, Sr, Ba, Y, Zr, Nb and Ta between experimentally produced amphiboles and silicate melts with variable F content, Chem. Geol. 109 (1993) 29–49.
[22] J.M. Brenan, H.F. Shaw, F.J. Ryerson, D.L. Phinney, Experimental determination of trace-element partitioning between pargasite and a synthetic hydrous andesitic melt, Earth Planet. Sci. Lett. 135 (1995) 1–11.
[23] T.Z. LaTourrette, R.L. Hervig, J.R. Holloway, Trace element partitioning between amphibole, phlogopite, and basanite melt, Earth Planet. Sci. Lett. 135 (1995) 13–30.
[24] M. Tiepolo, Determinazione sperimentale dei coefficienti di distribuzione solido/liquido in anfiboli di mantello: ruolo del controllo cristallochimico. Ph.D Thesis, Università di Pavia (1999) 315.
[25] K.H. Wedepohl, Die chemische Zusammensetzung der basaltischen Gesteine der nordlichen Hessichen Senke und ihrer Umgebung, Geol. Jb. Hessen 111 (1983) 261–302.
[26] G. Wörner, L. Viereck, J. Hertogen, H. Niephaus, The Mt. Melbourne Volvanic Field (Victoria Land, Antarctica) II. Geochemistry and Magma Genesis, Geol. Jb. 38 (1989) 395–433.
[27] L. Ottolini, P. Bottazzi, A. Zanetti, R. Vannucci, Determination of hydrogen in silicates by secondary ion mass spectrometry, Analyst 120 (1995) 1309–1313.
[28] P. Bottazzi, L. Ottolini, R. Vannucci, A. Zanetti, An accurate procedure for the quantification of rare earth elements in silicates, in: A. Benninghoven, Y. Nihei, R. Shimizu, H.W. Werner (Eds.), Secondary Ion Mass Spectrometry-SIMS IX, Wiley, New York (1994) 927–930.
[29] R. Oberti, L. Ungaretti, E. Cannillo, F.C. Hawthorne, The behaviour of Ti in amphiboles: four- and six-co-ordinate Ti in richterite, Eur. J. Mineral. 4 (1992) 425–439.
[30] F.C. Hawthorne, R. Oberti, A. Zanetti, G.K. Czamanske, The role of Ti in hydrogen-deficient amphiboles: sodic–calcic and sodic amphiboles from Coyote Peak, California, Can. Mineral. 36 (1998) 1253–1265.
[31] M. Tiepolo, A. Zanetti, R. Oberti, Detection, crystal–chemical mechanism and petrological implications of $^{[6]}Ti^{4+}$ partitioning in pargasite and kaersutite, Eur. J. Mineral. 11 (1999) 345–354.
[32] B.E. Leake, A.R. Woolley, C.E.S. Arps, W.D. Birch, M.C. Gilbert, J.D. Grice, F.C. Hawthorne, A. Kato, H.J. Kisch, V.G. Krivovichev, K. Linthout, J. Laird, J. Mandarino, W.V. Maresch, E.H. Nickel, N.M.S. Tock, J.C. Schumacher, D.C. Smith, N.C.N. Stephenson, L. Ungaretti, E.J.W. Whittaker, G. Youzhi, Nomenclature of amphiboles: report of the Subcommittee on amphiboles of the International Mineralogical Association Commission on new minerals and mineral names, Am. Mineral. 82 (1997) 1019–1037.
[33] A. Zanetti, R. Vannucci, R. Oberti, G. Dobosi, Trace-element compositions and crystal-chemistry of mantle amphiboles from the Carpatho–Pannonian Region, Acta Vulcanol. 7 (1995) 265–276.
[34] A. Zanetti, R. Vannucci, P. Bottazzi, R. Oberti, L. Ottolini, Infiltration metasomatism at Lherz as monitored by systematic ion-microprobe investigations close to a hornblendite vein, Chem. Geol. 134 (1996) 113–133.
[35] P. Beattie, On the occurrence of apparent non-Henry's law behavior in experimental partitioning studies, Geochim. Cosmochim. Acta 57 (1993) 47–55.
[36] T.H. Green, S.H. Sie, C.G. Ryan, D.R. Cousens, Proton microprobe-determined partitioning of Nb, Ta, Zr, Sr, Y between garnet, clinopyroxene and basaltic magma at high pressure and temperature, Chem. Geol. 74 (1989) 201–216.
[37] T. Andreessen, P. Bottazzi, R. Vannucci, K. Mengel, W. Johannes, Experimental determination of trace element partitioning between amphibole and melt, J. Conf. Abstr. V.M. Goldschmidt Conference 1 (1996) 17.
[38] M. Klein, H.-G. Stosch, H.A. Seck, Partitioning of high field-strength and rare-earth elements between amphibole and quartz–dioritic to tonalitic melts: an experimental study, Chem. Geol. 138 (1997) 257–271.
[39] R.D. Shannon, Revised effective ionic radii and systematic studies of interatomic distances in halides and chalcogenides, Acta Crystallogr. 32A (1976) 751–767.
[40] R. Oberti, R. Vannucci, A. Zanetti, M. Tiepolo, R. Brumm, On the correct calculation of amphibole/melt and amphibole/clinopyroxene D_{Ti} and their use in petrogenetic studies. Am. Mineral. (1999) in press.
[41] T.H. Green, Experimental versus Natural Two mineral Partition Coefficients - a 'High Teach' Controversy., Journal of Conference Abstracts, V.M. Goldschmidt Conference, Hidelberg, (1996) 213.
[42] P. Bottazzi, M. Tiepolo, R. Vannucci, A. Zanetti, S. Foley, R. Brumm, R. Oberti, Distinct site preference for heavy and light REE and the prediction of $^{Amph/L}D_{REE}$, Contrib. Mineral. Petrol. 137 (1999) 36–45.
[43] F.J. Ryerson, P.C. Hess, Implications of liquid–liquid distribution coefficients to mineral–liquid partitioning, Geochim. Cosmochim. Acta 42 (1978) 921–932.
[44] J. Blundy, B. Wood, Prediction of crystal-melt partition coefficients from elastic moduli, Nature 372 (1994) 452–454.
[45] K. Niida, D. Green, Stability and chemical composition of pargasitic amphibole in MORB pyrolite under upper mantle conditions, Contrib. Mineral. Petrol. 135 (1999) 18–40.
[46] S. Glaser, S. Foley, D. Günther, Trace element compositions of minerals in gernat and spinel peridotite xenoliths from the Vitim volcanic field, Transbaikalia, eastern Siberia, Lithos 48 (1999) 263–285.

[47] S. Foley, G. Wheller, Parallels in the origin of the geochemical signatures of island arc volcanics and continental potassic igneous rocks: The role of residual titanates, Chem. Geol. 85 (1990) 1–18.
[48] M. Defant, P. Richerson, J. De Boer, R. Stewart, R. Maury, H. Bellon, M. Drummond, M. Feigenson, T. Jackson, Dacite genesis via both slab melting and differentiation petrogenesis of La Yeguada volcanic complex, Panama, J. Petrol. 32 (1991) 1101–1142.
[49] M. Drummond, M. Defant, P. Kepezhinskas, The petrogenesis of slab derived trondhjemite-tonalite-dacite/adakite magmas, Trans. R. Soc. Edinb. Earth Sci. 87 (1996) 205–216.